Available online at www.sciencedirect.com
ScienceDirect
Physics Letters A 372 (2008) 1001–1008
PHYSICS LETTERS A
www.elsevier.com/locate/pla

Chaotic mixing enhancement in electro-osmotic flows by random period modulation

J. Rafael Pacheco [a,b,*], Kang Ping Chen [a], Arturo Pacheco-Vega [c], Baisong Chen [d], Mark A. Hayes [e]

[a] *Department of Mechanical and Aerospace Engineering, Arizona State University, Tempe, AZ 85287-6106, USA*
[b] *Flood Control District of Maricopa County, Phoenix, AZ 85009, USA*
[c] *CIEP-Facultad de Ciencias Químicas, Universidad Autónoma de San Luis Potosí, SLP 78210, Mexico*
[d] *Department of Mechanical and Aerospace Engineering, Jilin University, China*
[e] *Chemistry and Biochemistry Department & The Center for Solid State, Electronics Research, Arizona State University, PO Box 871604 Tempe, AZ 85287-1604, USA*

Received 6 March 2007; received in revised form 22 June 2007; accepted 28 August 2007

Available online 6 September 2007

Communicated by C.R. Doering

Abstract

In this Letter we report a method for enhancing mixing of a passive tracer in an electro-osmotic flow in a rectangular microchannel. A time-periodic electric field across the microchannel, filled with an electrolyte solution, is applied in order to realize a well-mixed state. A random perturbation to the time-periodic electric field is introduced in order to break the invariant tori of the system and achieve better mixing results. It is shown that under such period-modulation the enhancement effect increases with the strength of the modulation, and it is much reduced as diffusion is increased.

PACS: 47.61.Ne; 47.81.Lk; 47.52.+j; 47.51.+a

Keywords: Chaotic mixing; Electro-osmotic flow; Low Reynolds number; Random period modulation; Stochasticity

1. Introduction

In recent years, flow in microfluidic devices has become an active area of research. Current progress in fluid dynamics at the micro-scale level [1,2], and the development of miniaturized devices have been key factors in this increased interest. Microfluidic devices have been widely used in chemical processes [3,4], biomedical and pharmaceutical industries [5–8], aerospace technologies [9,10], electronic cooling [11–13], etc.

From the range of microfluidic devices developed up-to-date, considerable attention has been devoted to those using electrolyte solutions for rapid medical diagnosis and chemical and biological analyses, among other applications, since they offer advantages over pressure-driven flows [2,14–16]. Efficient mixing of reagents in these systems is often difficult to achieve because at small scales (typically < 100 μm), viscous effects are very important and force the system to operate in laminar regimes [17,18]. Under these circumstances, conventional techniques for mixing and transporting fluids, which require sufficiently large Reynolds numbers, become ineffective and/or complicated to use, and new alternatives are thus necessary.

Several passive [18–20] and active [21–23] mixers have been developed to achieve mixing in electro-osmotic flows in microchannels with encouraging results. In a previous work [24], a combination of steady and time-periodic electric fields across a microchannel filled with an electrolyte solution was proposed to realize a well-mixed state. The longitudinal steady electric field combined with constant surface electrical charges on both top and bottom walls, drive the primary flow in the

* Corresponding author at: Department of Mechanical and Aerospace Engineering, Arizona State University, Tempe, AZ 85287-6106, USA. Tel.: +1 480 965 8656.
E-mail address: rpacheco@asu.edu (J.R. Pacheco).

0375-9601/$ – see front matter
doi:10.1016/j.physleta.2007.08.051

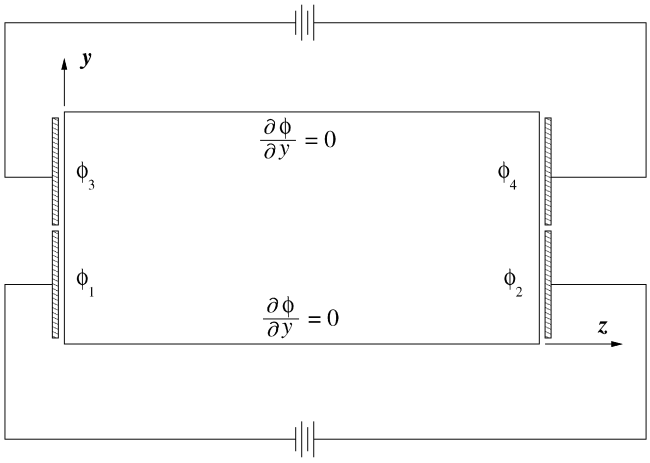

Fig. 1. Electrode arrangement for transverse electric field. A steady primary flow is in the x-direction perpendicular to the yz-plane.

longitudinal direction. In addition, secondary time-dependent external electric fields, orthogonal to the top–bottom steady fields, were applied along the side walls of the channel, as illustrated in Fig. 1, in an alternating on–off switching. It was shown that, as a consequence of this simple on-and-off periodic switching in the secondary transverse electric field, rapid and efficient mixing could be achieved. An advantage of this method, with respect to others proposed in the open literature, is that such operating condition could be implemented in practice by placing two micro-electrode pairs on the lateral walls of the channel (see Fig. 1), and turning on and off each electrode pair for one half period. To fully implement the aforementioned strategy, the effects of the side-walls of the channel cross section should be considered. Those effects were neglected in the slip-driven model of Pacheco et al. [24], which is valid so long as the Debye length is small compared to both (width and height) length-scales. Such limitation is removed in the present work and the exact three-dimensional electro-osmotic flow governing-equations, which include the effect of the electric double layers, are used to study the mixing process.

In this study we show that by introducing a random modulation of the transverse electric field, mixing of a passive tracer in an electro-osmotic flow through a microchannel can be improved. The successful application of stochasticity to break invariant tori (e.g., [25,26] to meso-scale flows) as well as resonant mechanisms to achieve uniform mixing (e.g., [27–29] in the context of micro-scale flows), have been prime motivations of the present analysis. When the applied electric field undergoes randomization, the Kolmogorov–Arnold–Moser (KAM) curves break up, the chaotic areas expand and the quasi-periodic areas shrink. This mixing effect becomes more noticeable as the strength of the perturbation and the period of the transverse electric field are increased. The numerical results presented here suggest that the effectiveness of this randomization protocol becomes less pronounced in the presence of strong diffusion.

2. Problem description

We focus on the analysis of a three-dimensional electro-osmotic flow in a long channel of rectangular cross section with height $2H$ and width $2W$.

The electrolyte solution is considered to be Newtonian and incompressible. The primary motion of the fluid is in the longitudinal direction of the channel (along the x-axis), driven by a constant electric field $\mathbf{E}_L$. The transverse motion of the fluid in the yz-plane is driven by a secondary electric field $\mathbf{E}_T(y,z,t)$ transverse to the primary flow direction. This flow is governed by the Navier–Stokes equations driven by electric body-forces with no-slip boundary conditions on the walls of the rectangular channel.

2.1. Governing equations

Assuming that: (i) the induced electric potential is small compared to the thermal energy of the ions and (ii) the electric double layer is thin, the governing equations in dimensionless form are given as

$$\nabla \cdot \mathbf{u} = 0, \tag{1}$$

$$Re(St\,\partial_t \mathbf{u} + \mathbf{u}\cdot\nabla\mathbf{u}) = -\nabla p + \nabla^2\mathbf{u} - K^2\psi(C_E\mathbf{i} - \nabla_\perp\phi - C_0\nabla_\perp\psi), \tag{2}$$

$$\nabla_\perp^2\psi = K^2\psi, \tag{3}$$

$$\nabla_\perp^2\phi = 0, \tag{4}$$

where $\mathbf{u}(x,y,z,t)$ is the nondimensional velocity vector, t is a dimensionless time, p is the normalized pressure, and ϕ and ψ are the normalized electric potentials due to an external electric field and due to the electric charge at the walls, respectively. In the set of equations, $Re = \rho U_c L_c/\mu$ is the Reynolds number, $St = L_c\omega/U_c$ the Strouhal number, $K^{-1} = (L_c\kappa)^{-1}$ is a dimensionless form of the Debye length, and $C_0 = \hat{\zeta}_0/L_c\hat{E}_0$. The constant $C_E = \hat{E}_L/\hat{E}_0$, on the other hand, is a quantity which measures the strength of the electric field along the channel $\hat{E}_L$, to that of the transverse field $\hat{E}_0$, and determines the residence time of the reagent.

The variables in Eqs. (1)–(4) have been scaled as follows: space variables by the characteristic length $L_c = 2H$, velocity components by the characteristic velocity $U_c = \epsilon\hat{E}_0\hat{\zeta}_0/\mu$, pressure by $\mu U_c/L_c$, electric potential $\hat{\psi}$ with $\hat{\zeta}_0$, electric potential $\hat{\phi}$ with $L_c\hat{E}_0$, time with $1/\omega$. The electrical permittivity of the solution is ϵ, $\hat{\zeta}_0$ is a constant zeta potential at the walls, and ρ and μ are the fluid density and viscosity, ω is a characteristic frequency of the transverse electric field, and κ^{-1} the Debye length (used to describe the thickness of the electric double layer). In Eq. (2) the last three terms in the right-hand side correspond, respectively, to the normalized axial electric field $\mathbf{E}_L$, the transverse field $\mathbf{E}_T(y,z,t) = -\nabla_\perp\phi$, with $\nabla_\perp = \mathbf{j}\partial/\partial y + \mathbf{k}\partial/\partial z$, and the induced electric field due to the zeta potential ψ. Note that the electric field and fluid flow equations are decoupled due to assumptions (i) and (ii) above. Thus, using the Debye–Huckel approximation, the electric potential $\psi(y,z)$ now satisfies a linearized form of the two-dimensional

Poisson–Boltzmann equation (3). On the other hand, the electric potential $\phi(y,z,t)$ can be obtained by solving Eq. (4) along with the boundary conditions of Fig. 1.

We can further simplify Eq. (2) by adding the $C_0K^2\psi\nabla_\perp\psi$ term to the pressure gradient to obtain a pseudo-pressure $\hat{p} = p - \frac{1}{2}C_0K^2\psi^2$. Thence, the transverse velocity field is solely a function of the potential ϕ, whereas the longitudinal electric field that drives the flow is a function of C_E alone. In the limit of small Reynolds number, the convective nonlinear term in the Navier–Stokes equations is negligible, and Eq. (2) is reduced to the following linear equation:

$$Re\,St\,\partial_t\mathbf{u} + \nabla\hat{p} = \nabla^2\mathbf{u} - K^2\psi(C_E\mathbf{i} - \nabla_\perp\phi), \tag{5}$$

where the unsteady term on the left-hand side of Eq. (5) is significant only for high-frequency unsteady flows.

Since the electro-osmotic flow considered here is solely driven by the electrical body force term in the right-hand side of Eq. (5), which can be computed independently of the velocity field, then we can decompose the velocity vector $\mathbf{u}$ into the sum of two contributions: the primary electro-osmotic flow along the longitudinal direction of the channel $\mathbf{u}_L = u(y,z)\mathbf{i}$, and the transverse flow $\mathbf{u}_T = v(y,z,t)\mathbf{j} + w(y,z,t)\mathbf{k}$, driven by the transverse electrical field. These two velocity fields are decoupled in the limit of small Reynolds numbers considered here, so that Eq. (5) can be re-written as

$$\frac{\partial\hat{p}}{\partial x}\mathbf{i} = \nabla_\perp^2\mathbf{u}_L - K^2\psi C_E\mathbf{i}, \tag{6}$$

$$Re\,St\,\partial_t\mathbf{u}_T + \nabla_\perp\hat{p} = \nabla_\perp^2\mathbf{u}_T + K^2\psi\nabla_\perp\phi. \tag{7}$$

Note that the velocity field is a function of y and z only.

The equations above have to be solved together with the continuity equation (1) for each velocity $\mathbf{u}_L$ and $\mathbf{u}_T$, and for the electrical potential equations (3) and (4), subject to no-slip boundary conditions for the velocity on all walls, given as

$$\begin{aligned} &y = 0, 1: \quad \mathbf{u}_L = \mathbf{u}_T = 0;\\ &z = 0, a: \quad \mathbf{u}_L = \mathbf{u}_T = 0, \end{aligned} \tag{8}$$

where $a = 2W/2H$ is the width-to-height aspect ratio, along with prescribed values of the electrical potential ψ on the walls:

$$\begin{aligned} &y = 0, 1: \quad \psi = 1;\\ &z = 0, a: \quad \psi = 0. \end{aligned} \tag{9}$$

2.2. Stochastic switching protocol

We now discuss the switching protocol that will make use of stochasticity to enhance the quality of mixing of this electro-osmotic flow. Due to the fact that the unsteady transverse flow $\mathbf{E}_T$ is a function of the electric potential ϕ, the linearity of the problem for ϕ allows us to write

$$\begin{aligned} \phi(y,z,t) = {}& \phi_1(t)F_1(y,z) + \phi_2(t)F_2(y,z)\\ &+ \phi_3(t)F_3(y,z) + \phi_4(t)F_4(y,z), \end{aligned} \tag{10}$$

where the functions $F_i(y,z)$, for $i = 1,2,3,4$, are solutions of the Laplace equation (4), with Dirichlet boundary conditions chosen such that $\phi_j = \delta_{ij}$; that is, the function F_1 is obtained from solving Eq. (4) with $(\phi_1,\phi_2,\phi_3,\phi_4) = (1,0,0,0)$, F_2 from the solution of Eq. (4) with $(\phi_1,\phi_2,\phi_3,\phi_4) = (0,1,0,0)$, and so on.

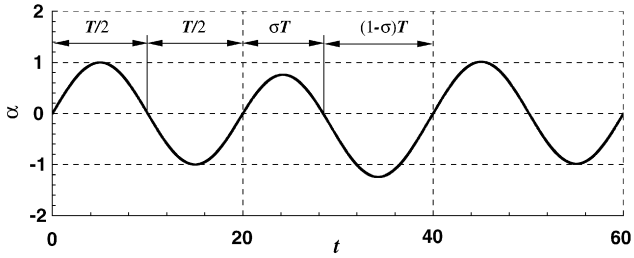

Fig. 2. Switching protocol α when random modulation is introduced. $T = 20$ and $\epsilon = 1$.

Following the strategy proposed in [24], we define the switching scheme in terms of amount of time the ϕ_i's (ϕ_1, ϕ_2, ϕ_3, ϕ_4) are on and/or off as follows: let $(\phi_1,\phi_2,\phi_3,\phi_4) = (0,1,0,0)$ for $\alpha > 0$, and then switch to $(\phi_1,\phi_2,\phi_3,\phi_4) = (0,0,1,0)$ for $\alpha < 0$, where α represents a time-like interval of variable length, and is defined as

$$\alpha = \sin\left(\frac{2\pi t}{T} \mp \gamma\right) \pm \varepsilon\beta. \tag{11}$$

In Eq. (11), β is a random number whose numerical value lies between ± 1 and acts as a vertical shift that modifies the values of α above and below zero, whereas $\gamma = \arcsin(\varepsilon\beta)$ is a phase shift as shown in Fig. 2. In the figure, the value of σ is related to the phase shift γ by $\sigma = 1/2 - \gamma/T$, and represents the fraction of the period T in which the value of $\alpha > 0$. By symmetry, an equivalent protocol could be applied reaching the same results by letting $(\phi_1,\phi_2,\phi_3,\phi_4) = (1,0,0,0)$ for $\alpha > 0$, and then switching to $(\phi_1,\phi_2,\phi_3,\phi_4) = (0,0,0,1)$ for $\alpha < 0$.

In the proposed scheme, we ensure that within the period T, ϕ_2 and ϕ_3 are on/off only once. This is achieved by setting the value of the shift $0 \leqslant \varepsilon \leqslant 1$. Clearly, a small value of ε will provide a small strength of the perturbation β. Also note that Eq. (11) does not modify the period T as shown in Fig. 2, and by setting $\varepsilon\beta = 0$ the boundary conditions for ϕ reduce to those of [24], i.e., ϕ_2 and ϕ_3 are on or off for half the period. As will be shown next, the key parameter for achieving chaotic mixing is demonstrated to depend on both the period T as well as the strength of the stochastic modulation $\varepsilon\beta$.

2.3. Convection-diffusion equation for the dispersion of a solute

The miscible dispersion of a solute into a flowing fluid in a non-uniform velocity field in a circular capillary was first analyzed by Taylor [30,31]. A slug of solute with a shape of a cylinder of the same diameter as the capillary was 'inserted' into the system while a solvent fluid was moving with a parabolic velocity profile. The major dispersion mechanisms for this problem were found to be both axial convection and radial diffusion. The problem studied here is slightly different from Taylor's; the solute initially is a small blob located at the center of the channel, instead of occupying the entire cross sec-

tion. The governing equation for the dispersion of a solute in a solution is the convection-diffusion equation. In dimensionless terms, this is given as

$$St\frac{\partial c}{\partial t} + \nabla \cdot (c\mathbf{u}) = \frac{1}{Pe}\nabla^2 c, \tag{12}$$

where c is the reagent concentration and $Pe = U_c L_c / D_m$, representing the ratio of the diffusion over the convection time scales, is the Péclet number and D_m is the mass diffusivity. For large Péclet numbers, convective-transport dominates over diffusive-transport. Thus, by promoting transport by convection, dispersion of the reagent in the flow field can be enhanced. In such diffusion-limited cases, the diffusion effects can be neglected, so that the reagent just convects with the fluid along the local instantaneous streamlines. Although much can be learned from the study of the trajectories of passive tracer particles, the results are only qualitative since diffusion is equivalent to adding noise to trajectories, which changes completely the nature of the system. Therefore, it is important to provide the information on the dispersion of the reagent in the flow field by solving Eq. (12).

2.4. Numerical methodology

Computer simulations of the flow in micro-scale systems enable easy control of the flow parameters and extensive data collection, while physical microchannel devices enable verification testing. In an experiment using an actual device, the microchannel gap is typically of the order of 100 μm or less, whereas the average velocity has a value of about 0.02 cm/s [32,33]. Electric fields can be generated using platinum electrodes placed on the sides of the walls taking the form of biased square waves. The periodic component of these waves, usually varies at frequencies between 0.5 Hz and 10 Hz. The kinematic viscosity of water ν at room temperate is approximately 10^{-6} m^2/s; thence the value of the Reynolds number ($Re = U2H/\nu$) is then about 0.04. For typical applications such as mixing in aqueous solutions, Péclet numbers in the range of $10 < Pe < 10^5$ are common, where the larger value corresponds to macromolecules such as proteins, as indicated by Stone et al. [34]. On the other hand, it is also important to note that in continuous-flow systems, the concept of distribution of residence times is relevant [35,36]. In the context of the present work, if the initial packets of reagent spread too much in the longitudinal direction then cross sectional mixing may be of little use. Thus, we calculate here the residence time as the time required for a reagent parcel to pass from the entrance to the exit of the microchannel. This residence time, RT, is then approximated as the ratio of the interior volume of the device to the flow rate of the passing solution. A typical value for a channel of length of 500 μm and an axial velocity of 2.0×10^{-7} m/s is $RT = 2500$ s.

To illustrate the promising features of this enhanced mixing approach, we consider typical values of the geometrical and physical parameters of the microchannel and the electrolyte solution, respectively, and use them along with the governing equations to study the mixing enhancement of this electro-osmotic flow when the proposed stochastic protocol is applied. Thus, the rectangular cross section of the channel is chosen to have an aspect ratio of $a = 2$. We set the dimensionless Debye length $K^{-1} = 0.01$, and the transverse electrical field parameter $C_E = 1/100$. The dimensions of the channel are $L_x = 5$, $L_y = 1$, $L_z = 2$. A $400 \times 120 \times 240$ grid mesh is used, respectively, in the x-, y-, and z-directions of the channel. Non-uniform grids, which are stretched away from the vicinity of the walls using a hyperbolic tangent function, are used in the channel cross section, whereas uniform grids are employed along it. The unsteady governing equations have been considered in a Cartesian coordinate frame and discretized on a staggered mesh by central second-order accurate finite-difference approximations. The resulting discretized system is then solved by a fractional-step procedure with the Poisson equation for pressure being inverted with a Multigrid method. The time advancement of the solution is obtained by a semi-implicit scheme with the Adams–Bashforth method for the explicit terms and the Crank–Nicholson method for the implicit ones as described in [37], where further details of the procedure can be found. We observed that twelve mesh points inside the Debye boundary layer were sufficient to achieve grid-independent results. The two-dimensional elliptic equations for ϕ and ψ were solved using the *FISHPACK* package [38]. During the computations the time step value was decreased to ensure time-independent results. In order to ensure the correct implementation of the numerical scheme previously mentioned, the velocity fields were compared to those obtained using a collocated arrangement of the variables on the grid, as described in [39–41], producing identical results.

3. Results and discussion

Results of the application of this randomization protocol on the mixing for systems with diffusion and for systems without diffusion are presented next.

3.1. System with negligible diffusion effects

In systems with no accountable diffusion, passive tracer particles move along the instantaneous streamlines downstream the channel; thus, chaotic dispersion can only occur in an unsteady flow field. In this negligible-diffusion limit, Eq. (12) reduces to a kinematic equation that can be written in a Lagrangian form to track the motion of a single tracer particle. This Lagrangian kinematic equation is

$$St\frac{\mathrm{d}\mathbf{r}}{\mathrm{d}t} = \mathbf{v}(\mathbf{r}, t), \tag{13}$$

where $\mathbf{r}(t) = x(t)\mathbf{i} + y(t)\mathbf{j} + z(t)\mathbf{k}$ is the location vector of the tracer particle, and $\mathbf{v}(\mathbf{r}, t)$ is the local velocity field. Computationally, $\mathbf{v}(\mathbf{r}, t)$ is obtained from a bilinear interpolation from the nodal values of the Eulerian velocity $\mathbf{u}(\mathbf{r}, t)$. Eq. (13) is then advanced in time from a given initial condition of the tracer particle position. The dynamical system given by Eq. (13) is numerically integrated using an adaptive Runge–Kutta scheme [42], so that errors in the trajectories of particles are mainly due

to discretization errors of the Eulerian velocity fields. The location of the particle at the end of each period is projected onto the yz-plane to generate the so-called Poincaré maps [43]. Although the reagent moves in a three-dimensional fashion, the flow is independent of the x-component, and as such, all the tools available to study two-dimensional flows are applicable to the analysis of this electro-osmotic flow. Following this idea, the Kolmogorov–Arnold–Moser (KAM) curves separate non-chaotic areas (islands) from chaotic ones. If tracer particles sample the entire cross section of the channel while moving downstream, i.e., if the Poincaré map covers the entire cross section, global chaotic mixing is then achieved. On the other hand, Poincaré sections produced by the numerical integration of Eq. (13) may produce spurious features, such as attractors if the incompressibility condition is not preserved. To minimize this potential problem, we have tested the numerical integration of the dynamical system Eq. (13) by reducing the time-step.

In order to provide random modulation of the period, we have to switch on and off the electrodes according to Eq. (11), i.e., let $(\phi_1, \phi_2, \phi_3, \phi_4) = (0, 1, 0, 0)$ for $\alpha > 0$, then switch to $(\phi_1, \phi_2, \phi_3, \phi_4) = (0, 0, 1, 0)$ for $\alpha < 0$. In what follows, we present the locations of 10 000 passive non-diffusive particles at $t = 500$ projected onto the yz-plane for various degrees of random period-modulation ε and periods $T = 3$, 10 and 20. The particles are initially located within a sphere of radius of 0.1 centered at $(x, y, z) = (1.0, 0.5, 1.0)$.

Fig. 3 corresponds to the results with period $T = 3$. As shown in Fig. 3(a), when there is no period-modulation, i.e., $\varepsilon = 0$, the tracer particles are tightly confined to the neighborhood of a well-defined symmetrical path, and there is hardly any mixing occurring in the cross section of the channel. As the period is randomly modulated with $\varepsilon = 0.1$, these particles spread to a wider region, as is evident from Fig. 3(b). Further increase in the strength of the period-modulation spread the particles to even larger and further areas in the channel cross section, an example of which is given in Fig. 3(c) for $\varepsilon = 0.5$. When the random perturbation strength reaches $\varepsilon = 1$, Fig. 3(d) shows that the particles nearly cover the entire yz-plane, and good mixing is achieved.

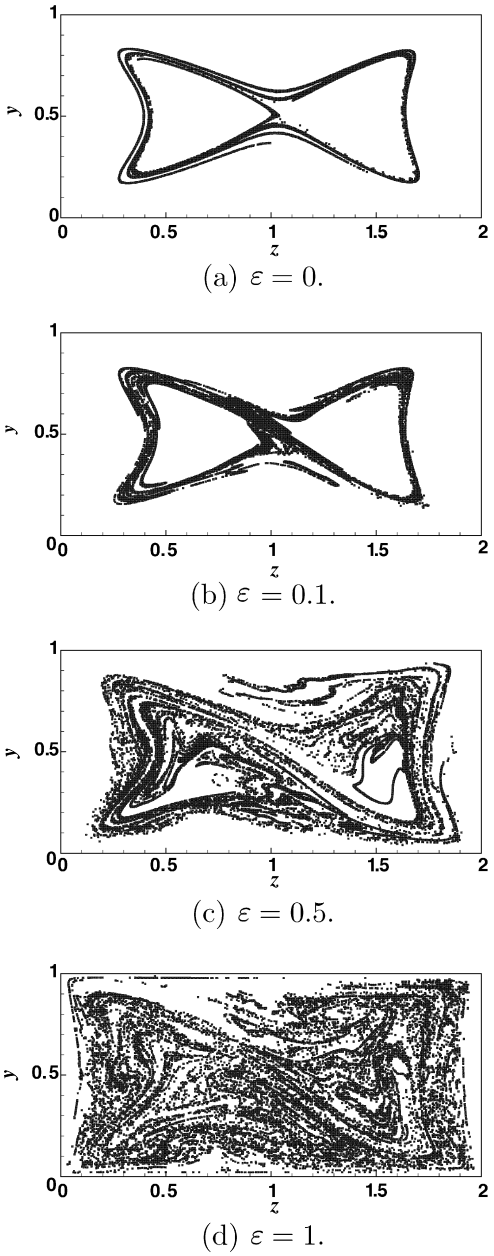

Fig. 3. Effect of period modulation on mixing of 10 000 non-diffusive particles for $t = 500$, $Re = 0.04$ and period $T = 3$.

The effect of random period modulation is shown for period $T = 10$ in Fig. 4. As in the previously discussed case, in the absence of period-modulation, $\varepsilon = 0$, there are two large holes near the center of the yz-plane, as illustrated in Fig. 4(a), where the particles cannot reach. As the period is randomly modulated with $\varepsilon = 0.1$, Fig. 4(b) shows that these unreachable islands become smaller and the particles spread into a much wider area in the cross section. When the modulation strength ε is increased to 0.5, these islands are nearly destroyed, and the particles are now able to reach most of the previously unreachable areas, as shown in Fig. 4(c). Finally, as was the case for $T = 3$, here a further increase in the modulation strength to $\varepsilon = 1$ also fills these holes with particles; though one can notice in Fig. 4(d) the presence of very small holes in the channel cross section because the particles are non-diffusive. Clearly stochasticity acts as an effective diffusivity on the particle trajectories [44]. Thus, a strategy to fill up all these smaller holes would be to stop the transverse motion and restart it after a short period of time.

This stochastically-modulated-period scheme is further tested for period $T = 20$ in Fig. 5. Clearly those areas unreachable when the period is not modulated, as seen in Fig. 5(a), can be reached with a random period-modulation, as shown in Figs. 5(b) and 5(c), where the increase in the modulation strength ε improves the quality of mixing dramatically. The random period-modulation acts as a random agitator on the passive particles and allows KAM curves to break. This stochastic agitation is similar to a cross sectional diffusive transport which intensifies as the modulation magnitude increases. Thus a strong random period-modulation greatly enhances mixing in these systems.

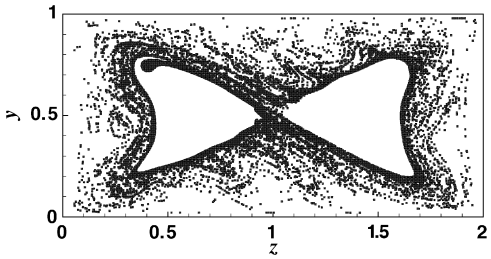

(a) $\varepsilon = 0$.

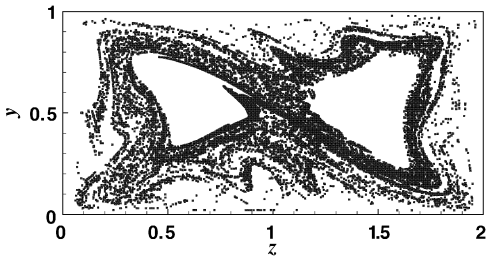

(b) $\varepsilon = 0.1$.

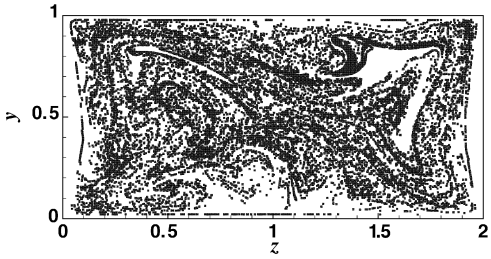

(c) $\varepsilon = 0.5$.

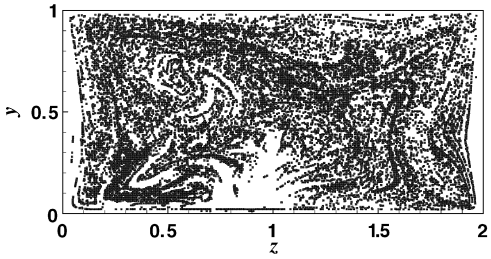

(d) $\varepsilon = 1$.

Fig. 4. Effect of period modulation on mixing of 10 000 non-diffusive particles for $t = 500$, $Re = 0.04$ and period $T = 10$.

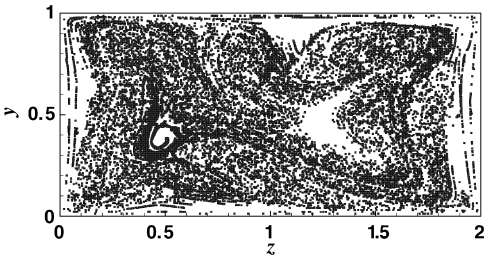

(a) $\varepsilon = 0$.

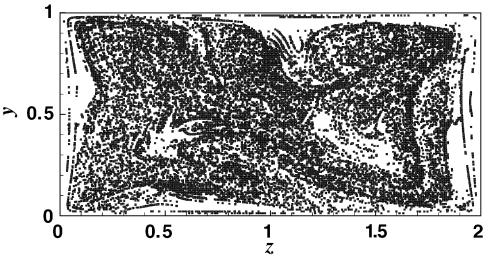

(b) $\varepsilon = 0.1$.

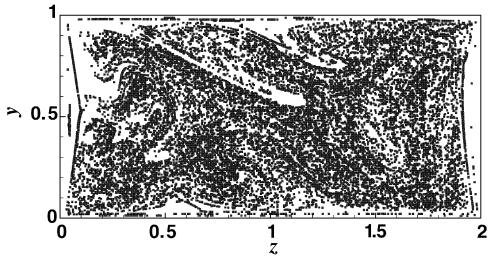

(c) $\varepsilon = 1$.

Fig. 5. Effect of period modulation on mixing of 10 000 non-diffusive particles for $t = 500$, $Re = 0.04$ and period $T = 20$.

3.2. System with accountable diffusion effects

A mixing measure that accounts for both diffusive and advective mixing effects can be defined by the normalized variance of the concentration [35,45], as

$$\Theta(t) = \frac{\langle c(\mathbf{x},t)^2\rangle - \langle c(\mathbf{x},t)\rangle^2}{\langle c(\mathbf{x},0)^2\rangle - \langle c(\mathbf{x},0)\rangle^2}, \tag{14}$$

where the spatial average $\langle\ \rangle$ in Eq. (14) is carried out over the entire domain. The quality of mixing Θ, is a positive function of time t, and its value approaches zero if the final state is uniformly mixed. The slope of the Θ curve is a measure of the rate at which particles in the solution mix; a steep drop in Θ is indicative of a fast mixing rate. To study the interplay between random period-modulation and molecular diffusion, we turn *off* the primary flow and the diffusion along the channel, and analyze the transverse-electric-driven flow in the two-dimensional cavity by means of the variance Θ.

For purposes of studying the time-scale to obtain a sufficiently homogeneous product, a circular blob of reagent of initial concentration $c_o = \langle c(y,z,0)\rangle = 1$, and radius 0.1, is centered at $(y,z) = (0.5,1)$. The quality of mixing Θ is then computed for Péclet numbers 10^4 and 10^5 by solving the convection-diffusion equation (12) for two different periods, $T = 10$ and $T = 20$ ($St = 0.6$ and $St = 0.3$). The Reynolds number is 0.04. The variance Θ is plotted as a function of time t for three cases: (a) pure diffusion (no fluid motion), (b) electro-osmotic motion and no period modulation, $\varepsilon = 0$; and (c) electro-osmotic motion and strong period modulation, $\varepsilon = 1$. In Figs. 6 and 7 the Péclet number Pe is set to 10^5 so that diffusive effects are weak when fluid motion is present. From the figures it can be seen that for pure diffusion, the value of Θ decays monotonically. When electro-osmotic motion is present, after the initial 10 time-units the value of Θ drops much faster than that of the pure diffusion case (keep in mind that a lower value of Θ indicates a more homogeneous state). The quality of mixing in Fig. 6 shows the effect of the stochastic period modulation protocol. The period modulation effect manifests itself when $t \gtrsim 100$ with an accelerated drop in the variance when

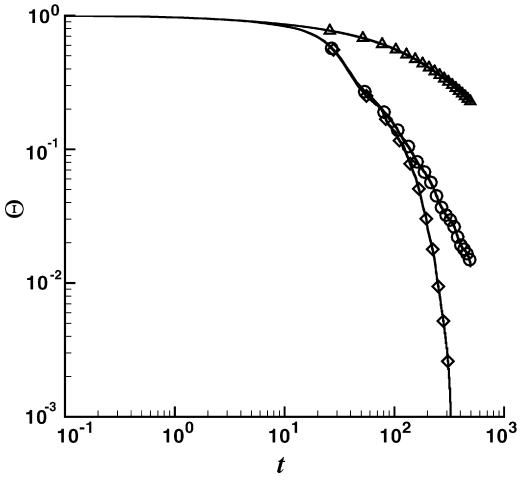

Fig. 6. Mixing quality Θ vs. time t, for $T = 10$; $Re = 0.04$ and $Pe = 10^5$. (△) Pure diffusion; (○) no period modulation; (◇) period modulation with $\varepsilon = 1$.

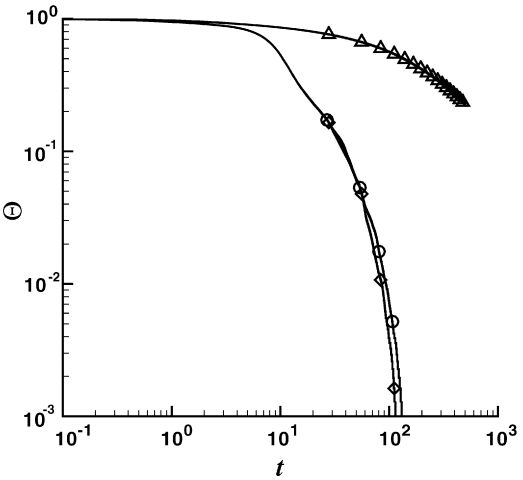

Fig. 7. Mixing quality Θ vs. time t, for $T = 20$; $Re = 0.04$ and $Pe = 10^5$. (△) Pure diffusion; (○) no period modulation; (◇) period modulation with $\varepsilon = 1$.

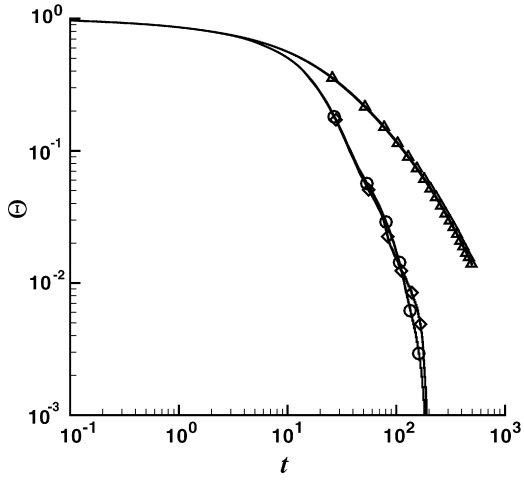

Fig. 8. Mixing quality Θ vs. time t, for $T = 10$; $Re = 0.04$ and $Pe = 10^4$. (△) Pure diffusion; (○) no period modulation; (◇) period modulation with $\varepsilon = 1$.

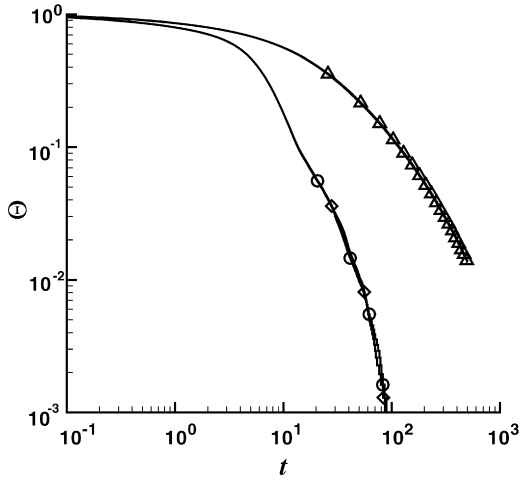

Fig. 9. Mixing quality Θ vs. time t, for $T = 20$; $Re = 0.04$ and $Pe = 10^4$. (△) Pure diffusion; (○) no period modulation; (◇) period modulation with $\varepsilon = 1$.

compared to the purely diffusive solution and to the stirring solution without such random perturbation. On the other hand, from Fig. 7 it can be seen that, when the period is increased to $T = 20$, the randomization protocol is less effective. The stochastic solution is essentially equivalent to the stirring solution with $\varepsilon = 0$, although both solutions beat the purely diffusive case. Since the shear in islands does enhance mixing over pure diffusion, it is possible that the size of the islands in the present case are small enough so that the effect of breaking them has little impact on the quality of mixing. Also note that the increase of the period T, acts as an artificial diffusivity for the fluid flow, and decreases the time needed to achieve a fairly homogeneous mixing.

In Figs. 8 and 9 the Péclet number Pe is set to 10^4 so that diffusive effects are stronger than the case analyzed above. The variance decay rate with and without stochastic modulation of the period are almost the same, suggesting that the modulation protocol is effective only above some threshold value of diffusion. It is evident by comparing the quality of mixing of Figs. 6 and 8, that the lower the value of Pe the lower the amount of time required to achieve a homogeneous mixing. A comparison of the rate of decay of the variance for $T = 10$ and $T = 20$ for a fixed Pe suggests that by increasing the period, a more efficient mixing will be obtained. Figs. 6–9 show that for $t > 10$ the quality of mixing $\Theta(t)$ decays exponentially with time. This decay has been observed and discussed previously by Pierrehumbert [25] and Antonsen Jr. et al. [46].

4. Summary

In this Letter, we have discussed the enhancement effect on mixing induced by a random period-modulation in an electro-osmotic flow of an electrolyte solution flowing inside a three-dimensional channel. The basic mechanics of stretching and folding of this active micro-mixer has been investigated using the concepts of Poincaré sections and quality of mixing. It has been shown that the degree of mixing as characterized by the Poincaré maps, and the quality of mixing Θ, increases with the

modulation strength. When the period is randomly modulated, the KAM curves break up, the chaotic areas expand and quasi-periodic areas shrink, thus providing a substantial enhancement in the mixing. It has also been shown that as the frequency of the transverse field decreases, the effectiveness of the random period-modulation becomes more pronounced and it is much reduced as diffusion is increased.

Acknowledgements

The authors thank Professors Y.-C. Lai, J.M. Lopez and A. Swimmer at ASU for their comments on the manuscript. The helpful comments of the anonymous referees, which have improved the quality of the manuscript, are very much appreciated. Computational resources for this work were provided by the Ira A. Fulton High Performance Computing Initiative at ASU.

References

[1] M. Gad-el-Hak, J. Fluids Eng. 121 (1) (1999) 5.
[2] T. Bayraktar, B. Srikanth, B. Pidugu, Int. J. Heat Mass Transfer 49 (2006) 815.
[3] T.S. Sammarco, M. Burns, AIChE J. 45 (2) (1999) 350.
[4] M. Losey, M. Schmidt, K. Jensen, Ind. Eng. Chem. Res. 40 (12) (2001) 2555.
[5] M. Burns, B. Johnson, S. Brahmasandra, K. Handique, J. Webster, M. Krishnan, T. Sammarco, P. Man, D. Jones, D. Heldsinger, C. Mastrangelo, D. Burke, Science 282 (1998) 484.
[6] H.-P. Chou, C. Spence, A. Scherer, S. Quake, Proc. Natl. Acad. Sci. USA 96 (1) (1999) 11.
[7] D. Dunn, I. Feygin, Drug Discovery Today 5 (12) (2000) S84.
[8] D. Beebe, G. Mensing, G. Walker, Annu. Rev. Biomed. Eng. 4 (2002) 261.
[9] M. Sen, D. Wajerski, M. Gad-el-Hak, J. Fluids Eng. 118 (3) (1996) 624.
[10] L. Lofdahl, M. Gad-el-Hak, Progress Aerospace Sci. 35 (2) (1999) 101.
[11] A. Weisberg, H. Bau, J. Zemel, Int. J. Heat Mass Transfer 35 (10) (1992) 2465.
[12] C. Harris, M. Despa, K. Kelly, J. Microelectromech. Syst. 9 (4) (2000) 502.
[13] X. Wei, Y. Joshi, IEEE Trans. Components Packaging Technol. 26 (1) (2003) 55.
[14] N.A. Patankar, H.H. Hu, Anal. Chem. 70 (9) (1998) 1870.
[15] M.J. Willey, A.C. West, Electrochem. Solid State Lett. 9 (7) (2006) E17.
[16] X. Chen, D.F. Cui, C.C. Liu, H. Li, J. Chen, Anal. Chim. Acta 584 (2) (2007) 237.
[17] A.D. Stroock, S. Dertinger, A. Ajdari, I. Mezić, H.A. Stone, G.M. Whitesides, Science 295 (2002) 647.
[18] T. Johnson, D. Ross, L. Locascio, Anal. Chem. 74 (2002) 45.
[19] T.J. Johnson, L.E. Locascio, Lab Chip 2 (2002) 135.
[20] R. Yang, C. Wu, T. Tseng, S.B. Huang, G. Lee, Jpn. J. Appl. Phys. Part 1 44 (10) (2005) 7634.
[21] A. Ajdari, Phys. Rev. Lett. 75 (1995) 755.
[22] A.D. Stroock, M. Weck, D.T. Chiu, W.T.S. Huck, P.J.A. Kenis, R.F. Ismagilov, G.M. Whitesides, Phys. Rev. Lett. 84 (15) (2000) 3314.
[23] S. Quian, H.H. Bau, Anal. Chem. 74 (2002) 3616.
[24] J.R. Pacheco, K.P. Chen, M.A. Hayes, Fluid Dyn. Res. 38 (8) (2006) 503.
[25] R.T. Pierrehumbert, Chaos Solitons Fractals 4 (1994) 1091.
[26] K. Ngan, T.G. Shepherd, J. Atmos. Sci. 56 (1999) 4134.
[27] T.H. Solomon, I. Mezić, Nature 425 (2003) 376.
[28] J.H.E. Cartwright, M. Feingold, O. Piro, J. Fluid Mech. 316 (1996) 259.
[29] I. Mezić, Physica D 154 (2001) 51.
[30] G.I. Taylor, Proc. Roy. Soc. A 219 (1953) 186.
[31] G.I. Taylor, Proc. Roy. Soc. A 223 (1954) 446.
[32] N. Polson, D. Savin, M. Hayes, J. Microcol. Sep. 12 (2000) 98.
[33] I. Glasgow, J. Batton, N. Aubry, Lab Chip 4 (2004) 558.
[34] H.A. Stone, A.D. Stroock, A. Ajdari, Annu. Rev. Fluid Mech. 36 (2004) 381.
[35] P.V. Danckwerts, Appl. Sci. Res. 3 (1952) 279.
[36] P.V. Danckwerts, Chem. Eng. Sci. 2 (1953) 1.
[37] J. Kim, P. Moin, J. Comput. Phys. 59 (1985) 308.
[38] P.N. Swartzrauber, SIAM J. Numer Anal. 11 (1974) 1136.
[39] Y. Zang, R.L. Street, J.R. Koseff, J. Comput. Phys. 114 (1994) 18.
[40] J.R. Pacheco, R.E. Peck, Numer. Heat Transfer B 37 (2000) 267.
[41] J.R. Pacheco, Int. J. Numer. Methods Fluids 35 (2001) 71.
[42] W.H. Press, B.P. Flannery, S.A. Teukolsky, W.T. Vetterling, Numerical Recipes in FORTRAN 77, The Art of Scientific Computing, second ed., Cambridge Univ. Press, Cambridge, 1992.
[43] J.M. Ottino, The Kinematics of Mixing: Stretching, Chaos and Transport, Cambridge Univ. Press, Cambridge, UK, 1989.
[44] A. Crisanti, A. Vulpiani, J. Stat. Phys. 70 (1993) 197.
[45] G.K. Batchelor, J. Fluid Mech. 5 (1959) 113.
[46] T.M. Antonsen Jr., Z. Fan, E. Ott, E. Garcia-Lopez, Phys. Fluids 8 (1996) 3094.